

Intense broadband THz generation from femtosecond laser filamentation

Tie-Jun Wang*, Shuai Yuan, Yanping Chen, and See Leang Chin

Centre d'Optique, Photonique et Laser (COPL) and Département de Physique, de Génie Physique et D'Optique, Université Laval, Québec, Québec G1V 0A6, Canada

*Corresponding author: tie-jun.wang.1@ulaval.ca; tjwang2007@yahoo.com

Received October 16, 2012; accepted November 16, 2012; posted online December 26, 2012

Broadband and energetic terahertz (THz) pulses can be remotely generated in air through filamentation. We review such THz generation and detection in femtosecond Ti-sapphire laser induced remote filaments. New results are presented on the direct relationship between THz generation in a two color filament and induced N₂ fluorescence through population trapping during molecular alignment and revival in air. This further supports the new technique of remote THz detection in air through the sensitive measurement of N₂ fluorescence.

OCIS codes: 140.3070, 190.5530, 350.5400.

doi: 10.3788/COL201311.011401.

1. Introduction

Terahertz (THz) wave is an electromagnetic radiation in the frequency interval between 0.1 and 10 THz. Compared to other frequency windows, THz has its special advantages for spectroscopy and imaging. For instance, from gighertz (GHz) to THz frequencies, numerous organic molecules exhibit strong absorption and dispersion due to rotational and vibrational transitions. These transitions are specific to the targets and enable THz fingerprinting in spectroscopy. THz waves can also penetrate many common materials such as paper, plastic, and ceramic, glass, wood, and clothes; THz has a low photon energy (4 meV @ 1 THz, one million times weaker than an X-ray photon) and will not cause harmful photoionization in biological tissues, etc. THz science and technology based on table-top laser system is finding use in an increasingly wide variety of important applications. With the rapid development of THz source technique, MV/cm level of THz field is available based on table-top laser system^[1]. High-field physics in the THz range becomes a very exciting frontier^[2–40].

However, the delivery of energetic THz pulses for spectroscopy at a remote position in the atmosphere is limited by linear diffraction and the strong attenuation due to water vapor absorption. THz generation from femtosecond laser remote filamentation in gases, especially in air, is a promising alternative because the technique allows the generation of intense near single-cycle THz pulses at a long distance by controlling the remote onset of the filament via controlling the initial laser parameters. Generation of intense THz pulses with large bandwidth from inside the filament in air is an active area of current research on THz science. Such broadband and rather powerful THz pulses would provide a new prospective tool for remote THz nonlinear optics and spectroscopy.

In this review, we briefly summarize the development of THz pulse generation from femtosecond laser-induced plasma filament, mainly from the experimental points of view, with emphasis on remote generation and detection

of high energy, broadband THz pulses. In particular, we shall present new results on the direct measurement of THz generation and N₂ fluorescence in a two color filament. Because of population trapping, the two signals followed each other during molecular alignment and revival in air. The results support the new technique of remote detection of THz pulses through the sensitive measurement of N₂ fluorescence as reported in Ref. [39,40].

2. THz generation from femtosecond laser filamentation

The first single-cycle THz generation from a photo-induced plasma was reported by Hamster *et al.* in 1993 by focusing laser pulses with a power of 1 TW and a duration of 100 fs into a He gas^[3]. The THz emission mechanism^[4] in their experiments was based upon space charge separation by the ponderomotive force generated by the optical beam, leading to a conical THz emission. Since then, other techniques have been used to generate intense THz emission. For example, by applying a transverse DC bias to the plasma region, an order-of-magnitude increase in the THz field was reported by Löffler *et al.*^[5,6]. Recently, Houard *et al.*^[7] and Chen *et al.*^[8] have applied external electric fields transversely to single-color filaments and Liu *et al.*^[9] have applied an external electric field longitudinally to single-color filaments. 3 orders enhancement of THz amplitude with up to 10 kV/cm external electric field has been reported^[7]. By applying a helical electrical field along a plasma region, Lu *et al.*^[10] could generate an elliptically polarized THz wave. An intense THz generation can also be generated from air plasma driven by an intense few-cycle laser pulse^[11,12]. The effect of the carrier envelope phase of few-cycle laser pulses on THz emission was predicted by Wu *et al.*^[11] and later on experimentally demonstrated by Bai *et al.*^[12].

A four-wave rectification method by focusing the fundamental wave (FW) and second-harmonic wave

(SHW) of an amplified Ti:Sapphire laser into air was reported in 2000 by Cook *et al.* to generate more than 3 orders stronger THz signal compared with only FW pumping^[13]. Since then, intense THz generations by the two-color pump have been investigated extensively. Bartel *et al.*^[14] reported THz electric field as high as 400 kV/cm and Kim *et al.*^[15] reported a super-broadband THz spectrum up to 75 THz ($\lambda=4 \mu\text{m}$) with μJ pulse energy. Dai *et al.*^[16] and Chen *et al.*^[17] demonstrated that THz emission from a two-color plasma filament could be amplified by another two-color plasma. The THz wave amplitude from a two-color filament can also be enhanced by more than eight times with an optimal aperture-limited pump laser beam according to Ref. [18] by Peng *et al.* Replacing the focusing lens with a gold off-axis parabolic mirror, Blanchard *et al.* reported more than 2 times increase in THz generation efficiency from two-color plasma^[19]. More recently, by using a converging lens followed by an axicon resulting in a tailored two-color laser filament in air, Manceau *et al.* reported significant THz temporal pulse shortening from a uniform plasma strings^[20]. The polarization of THz emission from a two-color filament in air can be coherently controlled by changing the optical phase between the FW and its SHW in air^[21] and Chen *et al.*^[22] or the surrounding gas pressure of two-color filaments^[23]. In the first case, the polarization could be rotated as reported by Dai *et al.*^[21] and Chen *et al.*^[22]. In the latter case, Manceau *et al.*^[23] observed both rotation and ellipticity change of THz polarization.

For the physical mechanism of the generation of THz pulses from two-color gas filaments, two theoretical models have been reported. The first model frequently used to explain THz emission is four-wave mixing (FWM)^[13,14,24,25] based on the third order non-linearity. The second is the microscopic polarization model^[15,26,27], also named photo-current model, which has been suggested to interpret the underlying dynamics, attributing the THz emission to the free-electron drift current driven by the combined field of the FW and its SHW. Both models describe the polarization and other properties of THz emission reasonably well^[21,22,25,28–30]. Recently, by applying an external DC electric field on a two-color filament in air, we found it could be reasonably concluded that THz emission from the two-color filamentation is mostly due to the FWM process, since the THz emission induced by an external DC field across the filament is mainly independent of the THz emission generated by the bichromatic excitation without the external DC field^[31]. A well-designed experiment is highly desired in order to distinguish between the two models.

3. Remote THz generation

An important reason why THz generation from femtosecond laser induced plasma filaments in air recently attracts much attention is that THz emission can be generated close to a remote target. Remote THz generation minimizes the importance of propagation issues as mentioned above. D'Amico *et al.* reported the first remote THz generation from the filaments induced by the FW of a Ti:sapphire based laser at a distance of 30 m from the laser in 2007^[32]. A radially polarized

forward conical emission was observed whose origin they attributed to a Cerenkov-type mechanism from the laser-pulse induced plasma wake. Their conclusion was based on the measurement obtained with a heterodyne detector (sensitive only to 0.1 THz with a bandwidth of 4 GHz). Later, by using an electro-optic sampling (EOS) technique (sensitive to frequencies below 4 THz), it was demonstrated by Chen *et al.*^[33] and Zhang *et al.*^[34] that the THz pulses in the forward direction of a filament were elliptically polarized. The physical mechanism is that filament induced birefringence in gases provides a phase delay between the two orthogonal components of the THz field, leading to an elliptically polarized THz emission. Liu *et al.*^[35] demonstrated that by sending a sequence of two femtosecond IR laser pulses at 800 nm separated by less than 3 ns, forming two overlapping filaments in air (so called bifilamentation), they can generate 1 order of magnitude more intense THz emission than the transient-Cherenkov THz emission^[32] from the plasma filament. The origin is attributed to the emission from a bimodal transmission line created by a pair of neighboring plasma filaments. Even so, the remotely generated THz pulse by femtosecond laser filamentation of the FW of a Ti:sapphire based laser system is still very weak (less than nJ/pulse).

For remote high energy, broadband THz generation, so far, two-color filamentation is strongly desired and is also challenging. Phase compensation between the two color beams is necessary so that the fundamental and second harmonic pulses overlap in the remote filament zone with parallel linear polarizations; this needs to be precisely controlled. One could set up a delay stage and a pair of ultra-thin wedges in one arm of the two-arm scheme (FW and SHW in each arm, respectively). However, fluctuation and mechanical instability would be serious in the two-arm scheme especially for long distance experiments according to our experience. Recently, an in-line phase compensation scheme was reported by Dai *et al.*^[21] to improve the stability. We adopted the setup in Ref. [21]

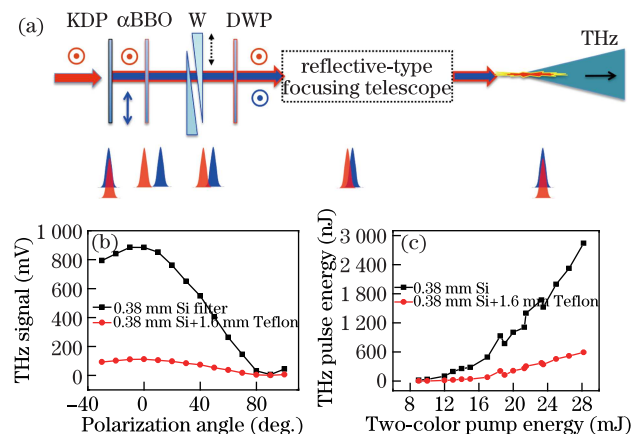


Fig. 1. (Color online) (a) Schematic setup for remote high energy THz generation. The pulses at the bottom indicate the time sequence of the two color beams. At a distance of 16 m, (b) THz pulse energy versus the polarization angle between the FW and the SHW and (c) THz radiation energy versus the input pump energy (two-color pump energy). In (b) and (c), solid squares and solid circles are filtered by 0.38 mm Si and 0.38 mm Si plus 1.6 mm Teflon, respectively transmitting THz frequency <300 THz and <5.5 THz.

together with a reflective-type telescope (Fig. 1(a)) to remotely generate high energy THz pulses in air^[36] using high energy large beam diameter (~ 30 mm) Ti-sapphire laser pulses. Here is a brief explanation of our design.

In order to decrease the nonlinear effects inside the optics of the in-line setup and also considering the large pump beam size, optics with large aperture had to be used. For frequency doubling, a 0.5-mm-thick KDP crystal with aperture >30 mm was chosen. At the output, for maximum conversion efficiency, the polarizations of the FW and SHW were orthogonal. When they passed through a birefringent crystal—X-cut α BBO with a clear aperture >30 mm, the FW was delayed compared to the SHW (so-called negative delay). All the following optics and propagation media (air) provided positive delays, which would result in the temporal overlap of the two pulses in a predetermined filament zone. A pair of ultrathin wedges (BK7, rectangular: 50×30 (mm), 4° wedge, angle, and 0.5 mm minimum thickness) could precisely control the relative phase between the two beams. A dual-wavelength wave plate (DWP) with a clear aperture of 30 mm rotated one of the polarizations by 90° and the other by 180° . The latter means that the polarization is un-affected. Thus, at the output of the DWP, the polarizations of the two pulses are parallel. A reflective-type telescope could project the two-color filament at a long distance. Its aberrations were minimized by using a concave off-axis parabolic reflector as a secondary mirror for the telescope. The THz radiation was collected and focused on a pyroelectric detector (Coherent P4-45CC) by a 90° off-axis, 4-inch in diameter Au-coated parabolic mirror. A 0.38-mm-thick 4-inch-diameter Si filter with another 0.5-mm-thick, 4×4 (mm) square Si-filter, stuck at the center of the former, were used to filter out the FW and SHW beams. The Si filter could transmit frequency <300 THz. Another 1.6-mm-thick Teflon was used as a long-pass wavelength filters to verify the spectral components (<5.5 THz) of the THz pulse. By minimizing the aberration of a telescope and optimizing the pump pulse duration^[37], the beam profile, the delay time and the polarization scheme between the FW and SHW pulses (Fig. 1(b)), a record pulse energy of $0.57 \mu\text{J}$ with frequency less than 5.5 THz and $2.8 \mu\text{J}$ for the entire super-broadband pulse (Fig. 1(c)) were measured at a ‘remote’ distance of 16 m^[36,38].

One can also remotely control this strong THz radiation by pre-aligned air molecules through rotational Raman excitation. During the filamentation of femtosecond laser pulses in air, most of the molecules survive in the plasma filament due to weak molecular ionization^[41]. However, the clamped intensity of $\sim 5 \times 10^{13}$ W/cm² in the filaments of the laser pulses is strong enough to align the neutral molecules through rotational Raman excitation, resulting in field-free periodic revivals. The typical revival periods of N₂ and O₂ molecules in air are 8.4 and 11.6 ps, respectively. Recently, Durand *et al.* reported a control of THz emission from bifilamentation of two FW pulses based on molecular lensing effect^[42]. The emission was characterized by a heterodyne THz detector, which was sensitive at 0.1 THz with a bandwidth of 4 GHz. Wu *et al.*^[43] and Wang *et al.*^[44] reported the molecular alignment effect on THz emission from two-color filaments in air. Air molecules were pre-aligned by the FW pulses^[43]

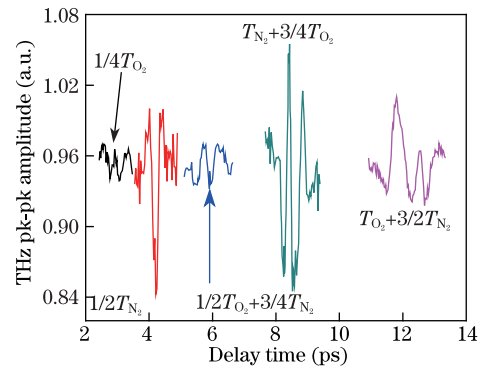


Fig. 2. (Color online) Experimental peak-to-peak amplitude of THz electric field as a function of delay time at each revival delay position of N₂ and O₂ including quarter, half, three-quarter, and full revival periods. T_{N_2} and T_{O_2} are typical revival periods of N₂ and O₂.

or a pair of two-color laser pulses^[44]. THz emission was generated by another pair of two-color laser pulses. By tuning the delay time between the alignment laser pulses and THz generating laser pulses around the air molecular revival time, significant modulations of the amplitude of the THz electric fields were observed. The peak-to-peak amplitude of THz electric field as a function of delay time is shown in Fig. 2 at each revival delay position of N₂ and O₂ including quarter, half, three-quarter, and full revival periods. The physics of this phenomenon will be given below in section 4.

More recently, a long distance dependence of remote THz generation from two-color filamentation in air was investigated by Daigle *et al.*^[45]. THz signals were still observed when the filaments were positioned 55 m from the source. But the results obtained revealed that as the filament bunch moved towards longer distances, the produced THz signal decreased monotonically. Through a simple numerical simulation the decaying mechanisms were identified as an eventually unavoidable group velocity mismatch between the two-color pulses and the diffraction/divergence of the non-filamenting second harmonic pulse^[45]. For example, assuming that both the pulses of FW and SHW had a pulse duration of 75 fs, the maximum interaction length of the two pulses was limited to 1.8 m according to the Eq. (7) in Ref. [45]. Any section of a filament whose length exceeded this value would not produce significant THz signal. Moreover, when the propagation distance increased, the intensity of the SHW pulse decreased due to its divergence. The production of strong THz pulses beyond 100 m from the current laser source is very challenging. A promising method to have strong THz generation beyond 100 m consists of increasing the clamped intensity by using a laser pulse with a longer wavelength since the generated THz field is proportional to the intensity of the FW pulse in FWM^[31]. Good beam profile, small F-number of focusing telescope beyond 100 m, and stable spatial and temporal control of two-color beam would also contribute to this remote THz generation.

4. Remote THz detection

Towards THz remote sensing, Prof. Zhang’s group recently introduced a technique for standoff THz wave

detection using the intrinsic physical properties of THz radiation enhanced emission of fluorescence (THz-REEF) from two-color laser-induced air plasma^[39,40]. The schematic setup is shown in Fig. 3^[40]. A two color laser beam (FW and its SHW) with parallel polarization was focused into air to generate a plasma with the relative phase being controlled by an in-line phase compensator^[21]. The initial input pulse energy of FW was 100 μJ . A single-cycle THz pulse with a peak field of 100 kV/cm, generated from a lithium niobate prism using a tilted pulse front scheme, was focused collinearly with the optical beam onto the plasma. The fluorescence emitted from the two-color laser-induced plasma was collected at a remote distance by a rotatable UV-enhanced concave mirror (M1) with a diameter of 200 mm and focal length of 500 mm, and was then guided by another UV plane mirror (M2) with a diameter of 75 mm through a monochromator into a photomultiplier tube (PMT). Coherent THz wave detection was achieved at a distance of 10 m by probing the independent THz pulses with a fully controllable, two-color laser-induced air plasma^[40].

The mechanism of THz-REEF from a plasma could be attributed to population trapping^[46–48] in the high-lying Rydberg states in molecules caused by intense two-color femtosecond laser pulses. Those trapped states could be ionized through collision with energetic electrons so as to form more ions. Also, the THz pulse could either further field ionize directly the trapped high-lying Rydberg states or heat the free electrons first which then impact-ionized these trapped states. The consequence was that the ion population was increased, which resulted in the enhancement of the fluorescence from the neutral N_2 molecules or molecular ions^[49]. The higher the THz field was, the stronger the fluorescence would be. Hence, the variation of the N_2 fluorescence follows the THz field variation. Since N_2 fluorescence in an air filament is in the UV and near UV (such as 337 and 391 nm)^[49], sensitive detection using PMT or ICCD would enhance the THz radiation significantly and could be applied to remote sensing.

We recently performed an experiment to confirm the above mechanism of enhancement of THz detection by looking simultaneously at the THz emission and the fluorescence, for example, at 337 nm of N_2 during molecular alignment and revival inside a filament in air. The

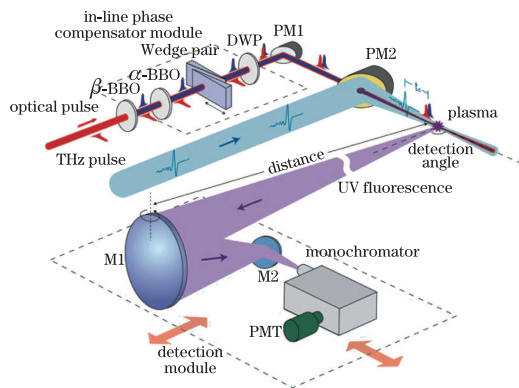


Fig. 3. (Color online) Schematic setup for THz wave remote sensing. Adapted from Liu *et al.*^[40].

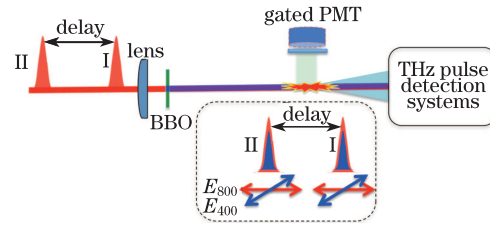


Fig. 4. (Color online) Schematic setup for molecular alignment control of THz and fluorescence generation. The inset shows the polarization and temporal schemes of two pairs of two-color pulses.

schematic setup is shown in Fig. 4.

Collinear laser pulses at a repetition rate of 1 kHz from beam I and beam II with precisely controlled delay time were focused by a 50-cm focal length lens and then passed through 0.1-mm-thick type-I-barium borate (BBO) crystal to produce second harmonic pulses. Pulse energies from beam I and beam II measured after the lens were 0.38 and 0.5 mJ, respectively. Through two-color filamentation in air, THz pulse was characterized by the electro-optical sampling (EOS) technique^[31]. The THz signal from beam II was optimized by varying the BBO angle which was then fixed. The optimum angle α between the optic axis and the FW's polarization direction was $\alpha \approx 55^\circ$ ^[44]. The linear polarizations and temporal schemes of the two pairs of two-color pulses after the BBO crystal are depicted as the inset of Fig. 4. The angle between the two polarizations of the FW and SHW was $\sim 35^\circ$. N_2 fluorescence at 337 nm was detected by a gated PMT covered by a 337-nm interference filter. In our experiments, the first pair of two-color laser pulses from beam I shown in the inset of Fig. 4 created filaments in air, resulting in the alignment and revival of air molecules. Since the SHW was around 2 orders of magnitude weaker than the FW, the FW played the dominant role in this molecular alignment event. The second pair of two-color laser pulses from beam II was used to generate THz pulses to probe/interact with the aligned and revived molecules. By scanning the relative delay time between the two pairs of pulses from beam I and beam II, THz electric field from the second pair of two-color pulses in the forward direction and the filament-induced 337-nm N_2 fluorescence from the side were measured (Fig. 4).

Figures 5(a) and (b) show the calculated response functions ($R(t)$) of the molecular rotational Raman effect (alignment and revival) in air created by the pulses from beam I as a function of delay time at half-revival of N_2 (Fig. 5(a)) and full revival of N_2 with three quarter revival of O_2 (Fig. 5(b)) given by the expression of $R(t) = n_{2,\text{rot}} \sum_{J=0}^{\infty} F_J \sin(-\omega_J t)$, where $n_{2,\text{rot}} = 32\beta^2(\omega)\pi^2 N/hcn_0$ is the overall magnitude of the rotational Raman effect, $\omega_J = 4\pi Bc(2J+3)$ is the angular frequency difference between the coupled rotational levels, B, N, h, c, n_0 , and $\beta(\omega)$ are the rotational constant of the molecule, the density of the considered gas, Planck's constant, the speed of light, linear refractive index at the laser wavelength, and the anisotropy of the molecular polarizability, respectively^[44]. $F_J = (\rho_{J+2} - \rho_J)Z_J(J+2)(J+1)/(2J+3)$ is a function of the transition moment between two coupled rotational levels ($J+2$ and J), of

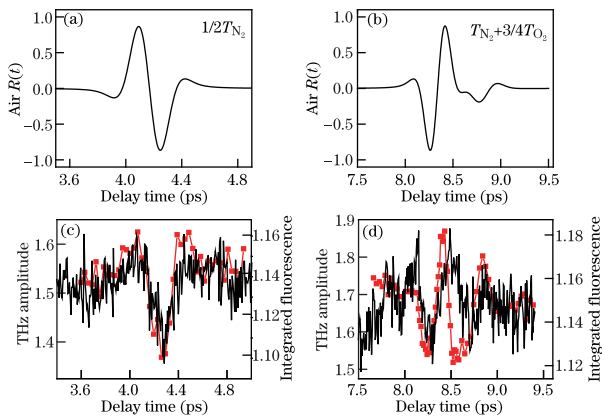


Fig. 5. (Color online) Calculated response function $R(t)$ of molecular Raman alignment in air (80% N_2 and 20% O_2) in (a), (b) and measured THz amplitude and 337 nm fluorescence as a function of delay time in (c), (d). (a) and (c) are for half-revival of N_2 , (b) and (d) are for full revival of N_2 and three quarter revival of O_2 .

the population difference ($\rho_{J+2} - \rho_J$) between these levels and of a weighting factor Z_J describing the multiplicity of each level. When the rotational Raman response function, $R(t)$, is >0 , the average molecular axis is parallel to the polarization of the exciting laser field and the refractive index change felt by another incoming laser pulse is positive^[50]. In our experiment, the exciting field is the 800-nm strong pulse in the first pair (I) of pulses in Fig. 4 and the so-called incoming pulse is the second pair (II) of pulses in Fig. 4. This would result in more focusing (guiding) of the second pair of pulses into the filament zone formed by the first pair of pulses. When $R(t)$ is <0 , the average molecular axis is perpendicular to the polarization of the exciting laser field and the refractive index change of the incoming laser pulse is negative.

The 337-nm fluorescence is proportional to the total number of N_2 ions which includes the ions in the ground state, N_2^+ , and in the excited states, N_2^{+*} ^[49]. The experimental observations of 337-nm fluorescence are shown at the half-revival time of N_2 in Fig. 5(c) and the full revival time of N_2 with three quarter revival of O_2 in Fig. 5(d). When the N_2 molecules are aligned parallel to the polarizations of the FW of beam I, both the FW and the SHW of beam II would experience an induced refractive index change which is positive^[50]. This corresponds to guiding (focusing), resulting in stronger filamentation, hence more ionization. This would give rise to more 337-nm fluorescence. At the same time, stronger THz pulses would be generated through FWM^[31]. These stronger THz pulses would ionize some of the trapped Rydberg states^[46–48] converging to N_2^+ and N_2^{+*} resulting in even more ionization, hence, more 337-nm fluorescence. When the aligned molecules are perpendicular to the polarizations of the FW and SHW, the induced refractive index change is negative^[50]. This corresponds to de-focusing, resulting in weaker filamentation. Weaker THz pulses will be generated through FWM. Thus, there would be less ionization of the trapped Rydberg states converging to N_2^+ , N_2^{+*} under weaker THz field, resulting in less 337-nm fluorescence. The consequence is that THz and fluorescence follow the alignment and revival; hence, follow each other. That is to say, when the THz field

is increased in a filament zone, the induced extra N_2 fluorescence also increases proportionately. This allows sensitive remote measurement using known sensitive optical detectors such as photomultipliers or ICCD.

5. Conclusion

In summary, we briefly review THz generation from femtosecond laser induced plasma filament. Since the THz source from filaments can avoid the propagation issues of diffraction and absorption, emphasis is put on the remote generation and detection of this high energy, broadband THz pulses. Towards remote high energy THz generation, THz pulses from two-color laser filamentation at a long distance are discussed; towards THz remote sensing, the technique of THz-REEF is reviewed. We also present new results on the direct relationship between THz generation in a two color filament and induce N_2 fluorescence through population trapping during molecular alignment and revival in air. This further supports the remote sensing technique of THz-REEF. We believe that by combining the techniques of the remote high energy broadband THz generation and the remote THz detection, broadband standoff THz spectroscopy is feasible.

This work was supported in part by NSERC, Canada Research Chair, the Canada Foundation for Innovation, the Canadian Institute for Photonics Innovation, and le Fonds Québécois pour la Recherche sur la Nature et les Technologies.

References

1. H. Hirori, A. Doi, F. Blanchard, and K. Tanaka, *Appl. Phys. Lett.* **98**, 091106 (2011).
2. R. Shimano, S. Watanabe, and R. Matsunaga, *J. Infrared Milli. Terahz. Waves* **33**, 861 (2012).
3. H. Hamster, A. Sullivan, S. Gordon, W. White, and R. W. Falcone, *Phys. Rev. Lett.* **71**, 2725 (1993).
4. H. Hamster, A. Sullivan, S. Gordon, and R. W. Falcone, *Phys. Rev. E* **49**, 671 (1994).
5. T. Löffler, F. Jacob, and H. G. Roskos, *Appl. Phys. Lett.* **77**, 453 (2000).
6. T. Löffler and H. G. Roskos, *J. Appl. Phys.* **91**, 2611 (2002).
7. A. Houard, Y. Liu, B. Prade, V. T. Tikhonchuk, and A. Mysyrowicz, *Phys. Rev. Lett.* **100**, 255006 (2008).
8. Y. Chen, T.-J. Wang, C. Marceau, F. Thériège, M. Châteauneuf, J. Dubois, O. Kosareva, and S. L. Chin, *Appl. Phys. Lett.* **95**, 101101 (2009).
9. Y. Liu, A. Houard, B. Prade, A. Mysyrowicz, A. Diaw, and V. T. Tikhonchuk, *Appl. Phys. Lett.* **93**, 051108 (2008).
10. X. Lu and X.-C. Zhang, *Phys. Rev. Lett.* **108**, 123903 (2012).
11. H.-C. Wu, J. Meyer-ter-Vehn, and Z.-M. Sheng, *New J. Phys.* **10**, 043001 (2008).
12. Y. Bai, L. Song, R. Xu, C. Li, P. Liu, Z. Zeng, Z. Zhang, H. Lu, R. Li, and Z. Xu, *Phys. Rev. Lett.* **108**, 255004 (2012).
13. D. J. Cook and R. M. Hochstrasser, *Opt. Lett.* **25**, 1210 (2000).
14. T. Bartel, P. Gaal, K. Reimann, M. Woerner, and T. Elsaesser, *Opt. Lett.* **30**, 2805 (2005).

15. K. Y. Kim, A. J. Taylor, J. H. Glowina, and G. Rodriguez, *Nat. Photon.* **2**, 605 (2008).
16. J. Dai, X. Xie, and X.-C. Zhang, *Appl. Phys. Lett.* **91**, 211102 (2007).
17. M.-K. Chen, J. H. Kim, C.-E. Yang, S. S. Yin, R. Hui, and P. Ruffin, *Appl. Phys. Lett.* **93**, 231102 (2008).
18. X.-Y. Peng, C. Li, M. Chen, T. Toncian, R. Jung, O. Willi, Y.-T. Li, W.-M. Wang, S.-J. Wang, F. Liu, A. Pukhov, Z.-M. Sheng, and J. Zhang, *Appl. Phys. Lett.* **94**, 101502 (2009).
19. F. Blanchard, G. Sharma, X. Ropagnol, L. Razzari, R. Morandotti, and T. Ozaki, *Opt. Express* **17**, 6044 (2009).
20. J.-M. Manceau, A. Averchi, F. Bonaretti, D. Faccio, P. Di Trapani, A. Couairon, and S. Tzortzakis, *Opt. Lett.* **34**, 2165 (2009).
21. J. Dai, N. Karpowicz, and X.-C. Zhang, *Phys. Rev. Lett.* **103**, 023001 (2009).
22. H. Wen and A. M. Lindenberg, *Phys. Rev. Lett.* **103**, 023902 (2009).
23. J.-M. Manceau, M. Massaouti, and S. Tzortzakis, *Opt. Express* **18**, 18894 (2010).
24. M. Kress, T. Löffler, S. Eden, M. Thomson, and H. G. Roskos, *Opt. Lett.* **29**, 1120 (2004).
25. X. Xie, J.-M. Dai, and X.-C. Zhang, *Phys. Rev. Lett.* **96**, 075005 (2006).
26. K. Y. Kim, J. H. Glowina, A. J. Taylor, and G. Rodriguez, *Opt. Express* **15**, 4577 (2007).
27. N. Karpowicz and X.-C. Zhang, *Phys. Rev. Lett.* **102**, 093001 (2009).
28. A. Houard, Y. Liu, B. Prade, and A. Mysyrowicz, *Opt. Lett.* **33**, 1195 (2008).
29. Y. Zhang, Y. Chen, S. Xu, H. Lian, M. Wang, W. Liu, S. L. Chin, and G. Mu, *Opt. Lett.* **34**, 2841 (2009).
30. D. Dietze, J. Darmo, S. Roither, A. Pugzlys, J. N. Heyman, and K. Unterrainer, *J. Opt. Soc. Am. B* **26**, 2016 (2009).
31. T.-J. Wang, C. Marceau, Y. Chen, S. Yuan, F. Théberge, M. Châteauneuf, J. Dubois, and S. L. Chin, *Appl. Phys. Lett.* **96**, 211113 (2010).
32. C. D'Amico, A. Houard, M. Franco, B. Prade, A. Mysyrowicz, A. Couairon, and V. T. Tikhonchuk, *Phys. Rev. Lett.* **98**, 235002 (2007).
33. Y. Chen, C. Marceau, W. Liu, Z.-D. Sun, Y. Zhang, F. Théberge, M. Châteauneuf, J. Dubois, and S. L. Chin, *Appl. Phys. Lett.* **93**, 231116 (2008).
34. Y. Zhang, Y. Chen, C. Marceau, W. Liu, Z.-D. Sun, S. Xu, F. Théberge, M. Châteauneuf, J. Dubois, and S. L. Chin, *Opt. Express* **16**, 15483 (2008).
35. Y. Liu, A. Houard, B. Prade, S. Akturk, A. Mysyrowicz, and V. T. Tikhonchuk, *Phys. Rev. Lett.* **99**, 135002 (2007).
36. T.-J. Wang, S. Yuan, Y. Chen, J.-F. Daigle, C. Marceau, F. Théberge, M. Châteauneuf, J. Dubois, and S. L. Chin, *Appl. Phys. Lett.* **97**, 111108 (2010).
37. T.-J. Wang, Y. Chen, C. Marceau, F. Théberge, M. Châteauneuf, J. Dubois, and S. L. Chin, *Appl. Phys. Lett.* **95**, 131108 (2009).
38. T.-J. Wang, J.-F. Daigle, S. Yuan, F. Théberge, M. Châteauneuf, J. Dubois, G. Roy, H. Zeng, and S. L. Chin, *Phys. Rev. A* **83**, 053801 (2011).
39. J. Liu and X.-C. Zhang, *Phys. Rev. Lett.* **103**, 235002 (2009).
40. J. Liu, J. Dai, S. L. Chin, and X.-C. Zhang, *Nat. Photon.* **4**, 627 (2010).
41. F. Théberge, W. Liu, P. Tr. Simard, A. Becker, and S. L. Chin, *Phys. Rev. E* **74**, 036406 (2006).
42. M. Durand, Y. Liu, A. Houard, and A. Mysyrowicz, *Opt. Lett.* **35**, 1710 (2010).
43. J. Wu, Y. Tong, M. Li, H. Pan, and H. Zeng, *Phys. Rev. A* **82**, 053416 (2010).
44. T.-J. Wang, S. Yuan, Z.-D. Sun, C. Marceau, Y. Chen, F. Théberge, M. Châteauneuf, J. Dubois, and S. L. Chin, *Laser Phys. Lett.* **8**, 295 (2011).
45. J.-F. Daigle, F. Théberge, M. Henriksson, T.-J. Wang, S. Yuan, M. Châteauneuf, J. Dubois, M. Piché, and S. L. Chin, *Opt. Express* **20**, 6825 (2012).
46. A. Talebpour, Y. Liang, and S. L. Chin, *J. Phys. B At. Mol. Opt. Phys.* **29**, 3435 (1996).
47. A. Talebpour, C. Y. Chien, and S. L. Chin, *J. Phys. B: At. Mol. Opt. Phys.* **29**, 5725 (1996).
48. S. L. Chin, A. Azarm, H. L. Xu, T. J. Wang, M. Sharifi, and A. Talebpour, in *Progress in Ultrafast Intense Laser Science (PUILS) VIII* K. Yamanouchi, M. Nisoli, and W. T. Hill, III, (eds.) (Springer, Berlin, 2012) chap. 4, p.79.
49. H. L. Xu, A. Azarm, J. Bernhardt, Y. Kamali, and S. L. Chin, *Chem. Phys.* **360**, 171 (2009).
50. F. Calegari, C. Vozzi, S. Gasilov, E. Benedetti, G. Sansone, M. Nisoli, S. De Silvestri, and S. Stagira, *Phys. Rev. Lett.* **100**, 123006 (2008).